Flight Test Evaluation of Precise Point Positioning Techniques Using Optical Ranging

Walton Williamson,* Bruce Haines,* Keith Wilson,† Joseph Kovalik,† Malcolm Wright,† Robert Meyer,* and Yoaz Bar-Sever*

ABSTRACT. — This article reports on a flight test for the purpose of validating single-vehicle Global Positioning System (GPS) precise point positioning (PPP) of an aircraft using JPL's Global Navigation Satellite System (GNSS)–Inferred Positioning System (GIPSY) software and postprocessed satellite products. The article provides a comparison of a laser ranging device to GPS position estimates relative to a fixed ground station. The range data derived independently from the laser and GPS techniques agree to an average of 6.6 cm (RMS). The flight test was conducted on a Cessna aircraft circling the laser ranging device installed at Table Mountain in Wrightwood, California, at a range of approximately 6 km while the aircraft flew at an altitude of about 4.3 km. An error budget is presented based on the GPS, laser, meteorology, and inertial sensors employed. The survey of the locations of the instruments and associated error is presented. The range error of 6.6 cm RMS is consistent with the error in the instruments and survey.

I. Introduction

The Jet Propulsion Laboratory (JPL) has developed a unique Global Positioning System (GPS) processing capability that enables high-accuracy position estimation and provides uniform, worldwide coverage. At the foundation of the JPL Global Differential GPS (GDGPS) system is a global network of geodetic-quality ground receivers, providing GPS code and carrier phase measurements continuously and in real time to JPL operations centers [1]. At three redundant operations centers, the measurements are processed using robust modeling and filtering algorithms in order to provide high-accuracy GPS satellite orbit and clock bias estimates. Accuracies of 20 cm are obtained in real time. To support the most demanding scientific applications, even higher accuracies (few cm) are available with longer latencies [2].

At the core of the processing systems is the Global Navigation Satellite System (GNSS)–Inferred Positioning System (GIPSY) software or its real-time counterpart, Real-Time GIPSY (RTG). This suite of software tools operates in the Linux environment and processes GPS data collected from a variety of applications in order to accurately geolocate both static and

* Tracking Systems and Applications Section.
† Communications Architectures and Research Section.

The research described in this publication was carried out by the Jet Propulsion Laboratory, California Institute of Technology, under a contract with the National Aeronautics and Space Administration.

dynamic GPS receivers, on the ground, in air, and in space. For instance, GIPSY supports radial orbit accuracies of better than 1 cm (RMS) with a latency of 4 hours when processing data from the Ocean Surface Topography Mission (OSTM) [3]. The high-accuracy estimates of GPS satellite orbits and clocks combined with high-fidelity models of the forces acting on the receiver satellites enable the high level of receiver accuracy. Recent advances in estimation have shown the ability to resolve the integer ambiguity between satellites and the ground-based GPS network of GPS receivers, enabling even higher levels of accuracy and confidence on receiver satellite orbital position estimates [4].

For real-time users, the GDGPS correction stream can be used to correct for errors in the broadcast GPS orbit and clock information. The RTG software can be optionally used to take full advantage of the GIPSY modeling and estimation capabilities in generating accurate, real-time position estimates. These capabilities have already been demonstrated for various airborne users [1]. This method requires that a vehicle such as an aircraft receive the real-time GDGPS corrections generated by JPL and transmitted to the vehicle via satellite or data link.

Recent tests comparing real-time (GDGPS) results with those from accurate (GIPSY-based) postprocessing have yielded differences of 10 cm (RMS) between the two methods [1]. However, both methods utilize the same fundamental GPS tracking observations. A method is desired that would provide an independent, external measure of the GPS-based positioning results.

To address this need, JPL has developed a laser ranging device referred to as the Aircraft Laser Uplink Ranging Experiment (ALURE). The system is capable of measuring the distance to an aircraft retroreflector from the ground with centimeter-level accuracies over distances of 10 km [5]. Using this approach to provide an independent validation of the GDGPS accuracy and GIPSY techniques to better than 10 cm should improve the confidence level of the GPS results.

This article reports on a flight test to demonstrate and independently validate high-accuracy GPS-derived airborne positioning. The primary technique for processing the GPS data from the flight tests is precise point positioning (PPP) using the GIPSY software. The overall solution strategy is discussed, and the results are compared to those from a short-baseline, kinematic technique, referred to as the annihilation method [6].

Using data collected from the flight test, we show that the measured difference between the ranges derived independently from the GPS and ALURE systems averages 6.6 cm (RMS). A discussion of experimental uncertainty shows that this measured error is consistent with the experimental uncertainty of approximately 7.7 cm (RMS).

II. GIPSY Precise Point Positioning

The PPP solution for terrestrial applications requires modeling and removal of a variety of GPS error sources. This section outlines the models utilized and provides a brief explanation of each. The results presented are generated using the highest-accuracy GPS satellite

orbit and clock products. These orbits have a 3D RMS accuracy of a few centimeters with a latency of 10 days [2].

Unmodeled GPS antenna phase variations (APVs) are possible sources of error. Antenna calibrations based on the International Global Navigation Satellite System (GNSS) Service (IGS) standard [7] were utilized in all GIPSY PPP processing to remove the intrinsic APV specific to each antenna model. The ground station was equipped with a geodetic choke-ring antenna (AOAD/M_T), while the aircraft utilized an Aerotech (AERAT2775_41) antenna. We note that the IGS antenna calibration models cannot account for the local multipath effects.

The GPS data were collected at the base station and aircraft at 1 Hz. The data were first edited for phase breaks and blunder points using the method described in [8]. The corresponding GIPSY software module (*ninja*) does not generate a position solution, but merely edits data on a per-satellite basis.

The editor also combines the L1 and L2 code and carrier phase observables to derive an ionosphere-free code and carrier phase measurement, eliminating the ionospheric delay errors to first order. These ionosphere-free measurements are processed within the estimation algorithms. In addition, the wide-lane data combination is formed to support resolution of the carrier phase ambiguities [4].

The aircraft flew at a range of 5 km laterally and 2 km vertically from the ALURE ground station. Over these distances (especially in the vertical), the troposphere errors are significantly different. The Vienna Mapping Function grid model [9] is utilized to provide the a priori dry and wet zenith troposphere delays as well as mapping functions (as a function of latitude and longitude) for both the aircraft and ground station. We used the model-generated values for both the dry and wet delays at a 1-Hz output, which is consistent with the data rate for the ground station and the aircraft.

For the static ground station, the zenith wet troposphere is estimated as a random-walk process with a time constant of 1 s and a process noise of 5.55e-6 ($cm/\sqrt{Hz}$). The aircraft utilized the zenith wet delay estimate from the VMF1 grid model at altitude. Unlike the ground station filter solution, the filter solution for the aircraft did not include an estimate of a zenith wet delay correction.

One important factor often overlooked is the use of solid-tide models. These models, such as the one described in the International Earth Rotation and Reference Systems (IERS) conventions [10], include the direct effects of the Moon and Sun, as well as ocean tidal loading, on the deformation of Earth's crust. The static base station is not truly static since the Earth's crust is slowly deforming due to solid tides, causing primarily altitude variations. When tide models are applied in GIPSY, this removes motion due to the Earth's crust and provides a static position in a tide-free system. During the experiment, however, the ground station was actually located between 12 to 27 cm above the static position realized using the tide-free convention. In order to compare the GPS calculated range to the laser range, the tide model corrections were thus added back to the static estimate of ground station location. This produces estimates for the true, instantaneous location of the ground GPS site

throughout the test flight. For the aircraft, we do not utilize a tide model since the vehicle is not sitting on the solid Earth.

Within GIPSY, a square-root information filter [11] performs forward filtering and backward smoothing of the GPS ionosphere-free carrier phase and pseudorange. The 3D position of the aircraft and the offset of the GPS receiver clock are estimated freely and independently at each 1-s data sample, with the only constraint coming from the uninterrupted accumulation of the carrier phase. Carrier phase ambiguities are resolved using a new single-receiver technique that relies on wide-lane information from regional fiducial GPS tracking stations [4]. (These stations participated in the global network solution underlying the high-accuracy GPS orbit products.) The filter process is restarted with constraints for the resolved integers to produce a refined estimate. While Table Mountain has a permanent geodetic-quality GPS station, it was not one of the regional fiducial sites used in producing the high-accuracy estimates of the GPS satellite orbits and clock offsets.

The GPS-calculated relative position is simply the difference between the static estimate of the base station (adjusted for the solid-tide motion) and the kinematic aircraft position. This difference is utilized for comparison with the ALURE measurement.

III. Comparison Kinematic Method

To provide a means of validation, results from a short-baseline kinematic carrier phase technique were compared to those from the GIPSY processing. This technique followed the method presented by [6]. The simple algorithm was implemented in Python and utilized as a quick reference for comparison. The algorithm proceeds in the following steps:

(1) L1 and L2 code and carrier phase measurements are collected from the static base station and the aircraft. Only those measurement epochs with six or more common satellites are considered. Satellites not observed commonly from both the ground and aircraft are removed.

(2) The static base station position is estimated using a simple least-squares algorithm and the GPS Broadcast Ephemeris at each epoch. This position provides the point of linearization for the rest of the algorithm.

(3) The VMF1 grid zenith dry and wet delays are utilized at both the base station and the aircraft to reduce the effects of troposphere. The Niell [12] mapping function is used to map the zenith delays to lines of sight to each GPS. This mix of models will be improved in future work.

(4) Wide-lane double-differenced carrier phase observables are formed using the L1 and L2 carrier phase data from the base station and the aircraft. Narrow-lane code observables are formed from the L1 and L2 code measurements. The differences between the narrow-lane and wide-lane residuals are utilized to estimate the integer ambiguity using a geometry-free method. The residuals were averaged over the time interval of interest (typically 10 min during a single pass of the aircraft around the laser) in order to form an initial estimate of the wide-lane integer ambiguity.

(5) Because of the proximity of the aircraft and ground receivers and because the differential troposphere was modeled, the primary error sources in the geometry-free residual are assumed to be receiver noise and multipath. The wide-lane carrier phase residual also has errors associated with the uncertainty in the relative position (which is large because ambiguities have not been resolved). The annihilator is formed to remove this error from the residual as shown in [6]. The new residual set is now considered a white-noise process with receiver noise and multipath modeled as Gaussian random variables.

(6) A set of wide-lane integers is hypothesized. A statistical hypothesis-testing scheme is utilized to estimate the probability that each hypothesis is correct given the residual history. The integers are considered fixed when the probability of a correct fix exceeds 99.9 percent.

(7) Once the wide-lane carrier phase integers are fixed, a least-squares algorithm is used to estimate the relative position at each epoch. This relative position can be compared against the laser or against the GIPSY solution.

The GIPSY method differs significantly from this short-baseline annihilation method. Tide models are not important to the annihilation method since the algorithm operates on the GPS measurements only. Only the relative position is estimated. However, the short-baseline method requires that a ground reference station be within a few kilometers of the aircraft in order to maximize the number of common satellites and minimize the effect of noncommon ionosphere and troposphere effects. GIPSY does not require common sets of satellites and estimates position in a common terrestrial reference frame. Ambiguity resolution in the annihilation method means resolving the double-differenced wide-lane integer ambiguity between the base station and aircraft. In GIPSY, wide-lane double-differenced integers are formed and resolved between the vehicle and nearby base stations used in a global network solution.

IV. ALURE

The ALURE system was developed at JPL for the purposes of providing short-baseline ranging and communication up to several kilometers. Details of the implementation may be found in [5].

A. ALURE Hardware

The ALURE optical ranging system has been modified slightly since the campaign described by [5]. Figure 1 shows an image of the ALURE telescope when looking at the installation from below. In Figure 1, the telescope is tilted on the gimbal to give a better perspective. The laser transmitter, involving a fiber Bragg grating, linewidth-narrowed, fiber-coupled, semiconductor 1064-nm diode laser, was externally modulated using the 100–Mbps pseudo-random bitstream (PRBS) data source. The polarized output was coupled into the three-stage Yb fiber amplifier and free-space coupled through an optical isolator to an SMF28 fiber for propagation to the telescope transmitter. Average output power was typically on the order of 2 W from the fiber.

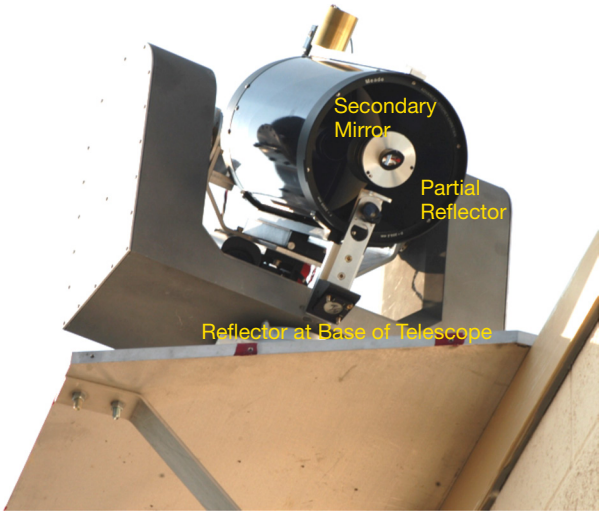

Figure 1. ALURE telescope on two-axis gimbal.

The ALURE transceiver, described previously [5], consists of a 20-cm Meade telescope and aspheric fiber collimator to launch the 2-mrad ($1/e^2$-diameter) output laser beam. Reflectors at the base of the telescope and in front of the secondary mirror direct to the beam to emit from the center of the telescope, allowing the returned signal to be centered on the telescope aperture. A 100-μm-thick optical window used a partial reflector in the transmitted beam path split off a small fraction to the receive detector to provide a local reference. The range was determined by differencing the reference signal from the target retroreflected signal. The receiver detector had a 100-MHz bandwidth and its output was sampled through an 8-bit digitizer.

The transceiver was mounted on a two-axis gimbal with a field of regard to the south and southwest of the Table Mountain Facility of about 150 deg. The 2-Hz range measurements were synchronized to a GPS receiver at 1 pulse per s (PPS) output.

B. Troposphere Correction for Lasers

Atmospheric propagation errors can cause significant light-time delays for the laser beam between the aircraft and ground station with the main contribution arising from the troposphere. The errors are effectively doubled since the laser passes through the same atmosphere twice. The Mendes-Pavlis [13] model was used to calculate the index of refraction associated with the lasers in this range of frequencies for given average temperature, pressure, and humidity. Measurements were made at the aircraft and at the ground station to compute the index of refraction at both locations. The average value of the two refractive indexes was used to correct the ALURE range measurement. A single index of refraction was calculated based on the measured profile, as noted below, and used to correct the ALURE measured range. No mapping functions were applied.

Balloon radiosondes launched before and after the flight provided a measurement of temperature, pressure, and humidity profiles. A single index of refraction (N = 1.000196)

was used, and is based on the average altitude of the aircraft/base-station pair. The total (two-way) delay between the aircraft and the ground station at a range of 5 km with 2 km altitude difference was on average 2.11 m of delay. The "dry air" contribution was on average 19.6 cm per km of range while the wet only contributed to 0.033 cm per km of range, which is effectively negligible.

The error in this estimate was calculated numerically using the Mendes-Pavlis model linearized around the value utilized and perturbed by the associated measurement uncertainties. The algorithm for generating the instantaneous refractive index is a nonlinear function of the local temperature, pressure, and humidity and includes assumptions on the local carbon dioxide environment [13]. An estimate of the error in the refractive index was calculated by perturbation methods. The partial of the refractive index with respect to each of the three instrument measurements (temperature, pressure, and humidity) was derived and then numerically computed, linearizing around the ground station instrument values. Calculation of the RSS error of the refractive index was then straightforward using the 1-sigma uncertainty in each of the three instruments. The RSS error of the independent contribution of each measurement (temperature, pressure, and relative humidity) created an uncertainty of 0.46 cm per km of error. The total contribution to error at a 5-km range with 2-km altitude difference was estimated at 2.49 cm in range (one-way). Therefore, index of refractivity estimate error contributed 2.49 cm in range to the overall error budget.

V. Experiment Configuration and Uncertainty

The experiment consisted of two segments: the aircraft and the ground station. Errors associated with each of these segments are presented. The error uncertainty is then assessed for the GPS and ALURE solutions to form a total expected experimental error.

A. Aircraft

The aircraft was a Cessna 206 and flew from Bob Hope Airport in Burbank, California, to Table Mountain during the 4-hour flight experiment. The aircraft was equipped with a periscope primarily used for aerial photography. The periscope is fixed to the aircraft body frame, but free to rotate about the aircraft Z-axis when manually adjusted. The periscope was fitted with a corner-cube retroreflector and the angle of rotation was fixed to +10 deg about the aircraft positive Z-axis (down). The orientation at 0 deg of rotation was such that the corner cube faced directly to starboard.

The aircraft was fitted with a GPS receiver, inertial measurement unit (IMU), and air data system. Figure 2 shows the block diagram of the primary instruments utilized. The primary GPS antenna used for the experiment was an Aerotech AT2775-41W with 26 dB of gain. It was mounted on the fuselage just above the cockpit. Calibrations for the antenna phase variations were made according to the IGS standard [7].

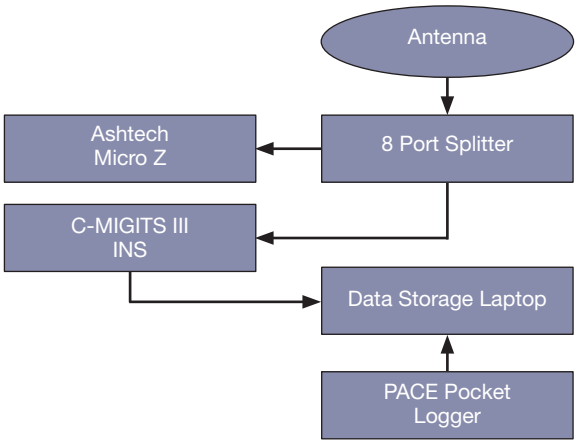

Figure 2. Aircraft GPS and INS instrumentation block diagram.

The primary antenna was connected to an Ashtech Micro-Z L1/L2 geodetic-quality receiver through a splitter. The Ashtech was used as the primary data source for the GPS data presented in this article. It provided measurements of L1 and L2 carrier phase as well as coarse/acquisition (C/A), P1, and P2 code (pseudorange).

Attitude was measured in flight using a Systron Donner C-MIGITS III inertial navigation system (INS). The C-MIGITS has an L1-only receiver, which was connected to the same primary antenna through a splitter. The C-MIGITS provided estimates of heading, pitch, and roll in order to relate the position of the primary antenna to the position of the retroreflector in flight.

A survey was performed of the aircraft prior to flight using a Leica Total Station (LTS). This station has the ability to define a common reference frame and measure distances in that reference frame to better than 1 mm per axis (RMS) using its own laser ranging device. The LTS laser is compatible with the retroreflector, enabling precise position estimates of the reflector center. The C-MIGITS was mounted to an aluminum plate with corner-cube reflectors. This plate defined the reference frame for the aircraft. The C-MIGITS was precisely mounted to the plate by lab technicians with submillimeter accuracy. Therefore, measured vector lever arms from the mounting plate to the primary GPS antenna and the retroreflector were defined in a coordinate frame defined by the attitude of the C-MIGITS IMU. This coordinate frame is referred to as the aircraft body frame.

The lever arm from the GPS antenna phase center to the retroreflector is calculated using the survey data and the inflight data. It is represented as L^E_{F2ref} and is defined in the Earth-centered, Earth-fixed (ECEF) frame when compared to the ALURE range and GPS position. This lever arm is made of the following components:

$$L^E_{F2ref} = C^E_{NED} C^{NED}_B \left(L^B_{FPC} + L^B_{F2refcor} + C^B_{ref} L^B_{ref} \right)$$

The term C^E_{NED} is the rotation matrix from the north–east–down (NED) reference frame to the ECEF frame and is calculated using the instantaneous latitude and longitude of the vehicle. The term C^{NED}_B is the rotation matrix from the aircraft body frame to the NED frame

and is calculated using the C-MIGITS heading, pitch, and roll estimates. The lever arm L^B_{FPC} is the vector from the Aerotech antenna phase center (for the ionosphere-free GPS observable) to a physical antenna reference point (ARP), and is derived from the antenna calibration information [7]. The lever arm $L^B_{F2refcor}$ is the vector from the ARP to the center of rotation for the periscope. The lever arm L^B_{ref} is the vector from the center of rotation to the retroreflector phase center with the rotation matrix C^B_{ref} defining the rotation of the periscope relative to the aircraft body frame.

A first-order error analysis of the effect of uncertainty in this lever arm to the total range is calculated using the LTS estimated error of 1-mm error per axis in the measured distance of each lever arm. The error in the rotation from the NED frame to ECEF is assumed negligible. If a 0.5-deg heading error and 0.1-deg pitch and roll errors are assumed, the total contribution of error over the surveyed distance of 1.67 m from the GPS phase center to the ALURE retroreflector is about 1.8 cm (RMS) of uncertainty in range.

B. Ground Station

The ground station consists of the GPS antenna and receiver located next to the ALURE laser, as shown in Figure 3. A survey was performed to determine the distance from the ALURE transmission point to the phase center of the GPS antenna. The measurement is defined in the following equation:

$$L^E_{Grnd} = C^E_{NED} C^{NED}_L \left(C^L_{gim} L^{gim}_{TL} + L^L_{LG} + L^L_{GPC} \right)$$

The arm defines L^E_{Grnd} as the distance from the ALURE transmission point to the GPS phase center in the ECEF frame. The lever arm L^{gim}_{TL} represents the surveyed vector from the transmission point to the center of rotation of the ALURE gimbal. The rotation matrix C^L_{gim} represents the rotation from elevation and azimuth of the gimbal to the local tangent frame L.

Figure 3. GPS choke-ring antenna installed next to ALURE at the Table Mountain facility.

The lever L_{LG}^{L} is the surveyed vector from the ALURE gimbal center of rotation to the GPS ARP. The L_{GPC}^{L} represents the rotation from the ARP to the GPS phase center as provided in the antenna calibration data [7]. The rotation matrix C_{L}^{NED} represents the rotation from the local tangent frame defined by the survey into the NED frame. The LTS defined the reference frame relative to the local gravity and magnetic north.

A complex method of combining the GPS and the total station was utilized to estimate the rotation C_{L}^{NED} in the NED frame. The LTS measured the position of the Optical Communications Telescope Laboratory (OCTL) GPS antenna. The LTS also measured the center of rotation of the ALURE and the orientation of the ALURE relative to the local gravity field. A second GPS receiver/antenna combination was placed on the ground about 14.5 m from the building. The LTS measured the location of the second GPS antenna in the same reference frame as the primary GPS and the ALURE. GIPSY provided a differential GPS solution between the primary GPS receiver on the wall next to the ALURE and the second receiver on the ground. This relative GPS position was utilized to define an angle relative to north from the primary to secondary GPS receiver. Since the LTS put the two GPS antennas and the ALURE into a common reference point, a transformation was derived to determine the ALURE location and orientation in the NED frame. When the ALURE gimbal pointed at 0 deg of elevation and azimuth angle, its heading faced 229 deg from north. Assuming a 1-mm total station error and a 0.5-cm GPS lever arm error per axis, the total expected error in the angle from north was 0.65 deg, resulting in a range uncertainty of less than 4.0 cm.

The total vector range from the ALURE transmission point to the GPS phase center was measured to be 2.81 m. The estimated error in the lever arm L_{Grnd}^{E} in the ECEF frame is 4.6 cm. This value assumes a 1-mm per axis error in the survey, a 0.05-deg (1-sigma) angle uncertainty in the gimbal encoder angles, a 0.1-deg uncertainty in the local tangent pitch and roll, and a 0.5-deg uncertainty in the estimation of the true north from the magnetic north. Other than the instruments, this uncertainty in the local tangent frame contributes the most to the overall error.

C. ALURE Range Uncertainty

The primary error sources in the laser ranging reference system are the laser range measurement and uncertainty in modeling of the troposphere. In order to estimate the uncertainty in the ALURE range, a static retroreflector was placed approximately 1 km from Table Mountain on the other side of the valley. Repeat-pass calibrations yielded range variations of less than 4 mm during calibration.

The range was corrected for troposphere error as shown below, where N is the computed index of refraction, c is the speed of light and $\tau_f - \tau_0$ represents the total measured time difference between when the signal was emitted and when it was received:

$$\Delta R_{LLR}^{gim} = \frac{c(\tau_f - \tau_0)}{2N}$$

An index of refraction (N=1.000184) corresponding to the average altitude of the aircraft/base-station pair was determined on the basis of a weather balloon profile. As stated previ-

ously, the estimated total uncertainty in these measurements limited the estimated accuracy of the index of refraction to ±4.6 parts per million. At the estimated range, this contributes 2.49 cm of uncertainty (one-way).

D. GPS Uncertainty

The goal of this article is to assess the uncertainty in the GPS PPP solution using the laser. However, for the purposes of assessing the limits of the experimental uncertainty, the GPS uncertainty is assumed to be consistent with previously published real-time estimates (from GDGPS) and the postprocessed solutions [1].

The GPS receiver relative position estimate is represented by $\Delta P^E_{GF} = P^E_F - P^E_G - PP^E_{tide}$, where the aircraft estimate at the GPS antenna phase center is represented by P^E_F in the ECEF frame, the static base-station position of the phase center is represented by P^E_G in the (tide-free) ECEF frame, and P^E_{tide} represents the time-varying solid-Earth tide correction for the static base station estimated using the solid-Earth tide model [10].

The previously established error between the PPP solution and the real-time (GDGPS) methods is approximately 10 cm 3D RMS [1]. Projecting this error along the line of sight to Table Mountain results in an estimate of only 5.77 cm to the error in the range comparison with the ALURE.

E. Range Comparison

Ultimately, the goal is to compare the ALURE range with the GIPSY computed differential range. The range measured by the ALURE should equal the range difference between the GPS antennas after adjusting for the lever arms, as shown in the following equation:

$$\left\|\Delta R^{gim}_{LLR}\right\| = \left\|L^E_{Grnd} + \Delta P^E_{GF} + L^E_{F-ref}\right\|$$

In this case, the term ΔR^{gim}_{LLR} is the ALURE range (corrected for troposphere) from the transmission point on the gimbal to the reflector on the aircraft. The lever arms were defined previously. Table 1 summarizes the uncertainty for all measurements listed. Error components were assumed independent of each other. Therefore, the total is the root-sum-square (RSS) of the error sources and represents a 1-sigma uncertainty. The total expected experimental uncertainty is 7.73 cm (RMS).

Table 1. Summary of component errors and total experimental uncertainty.

Parameter	Uncertainty, cm
GPS	5.77
Laser	2.67
Lever Arms	4.39
Total	7.73

VI. Flight Test Results

The flight was conducted in the early morning of February 26, 2010. During the flight test, the aircraft orbited the Table Mountain facility numerous times. The ALURE laser was able to track returns from the aircraft during four passes. Figure 4 shows the difference between the range calculated by the ALURE and the GPS. The visible gaps in the data set represent portions of the orbit where the aircraft was outside of the field of regard of the ALURE transceiver. Errors were bounded by +10 cm to –15 cm.

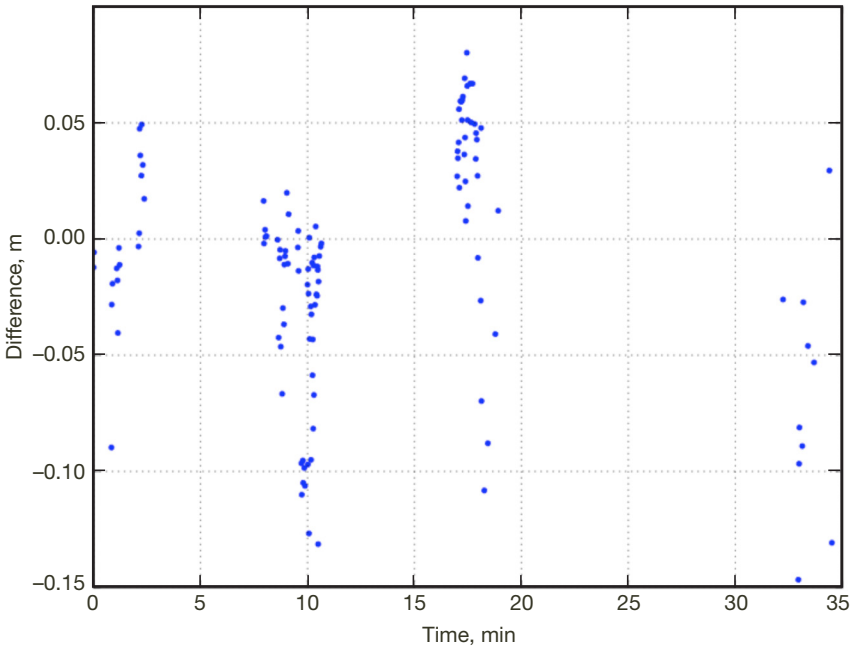

Figure 4. Difference between GPS and ALURE range estimates.

Figure 5 shows a close-up of a typical track from the fourth pass. In this case, the gaps in data represent the points at which the ALURE did not receive a signal return from the retro-reflector.

Table 2 shows the mean, standard deviation, and RMS error in centimeters for all four track passes. The average RMS error over all four runs is 6.6 cm.

On track number 8, the ALURE signal-to-noise ratio on returns began to drop significantly and the laser suffered a failure shortly thereafter. This loss of function may have added to the uncertainty in the final run.

Over the period of test, the GIPSY solution was compared with the annihilation short-baseline technique presented previously. Figure 6 shows the vertical difference. Table 3 shows the difference in the solutions in the NED frame during run 4. The correlation of these two methods is consistent with errors reported both with the GDGPS results [1] and previous formation flight experiments [14].

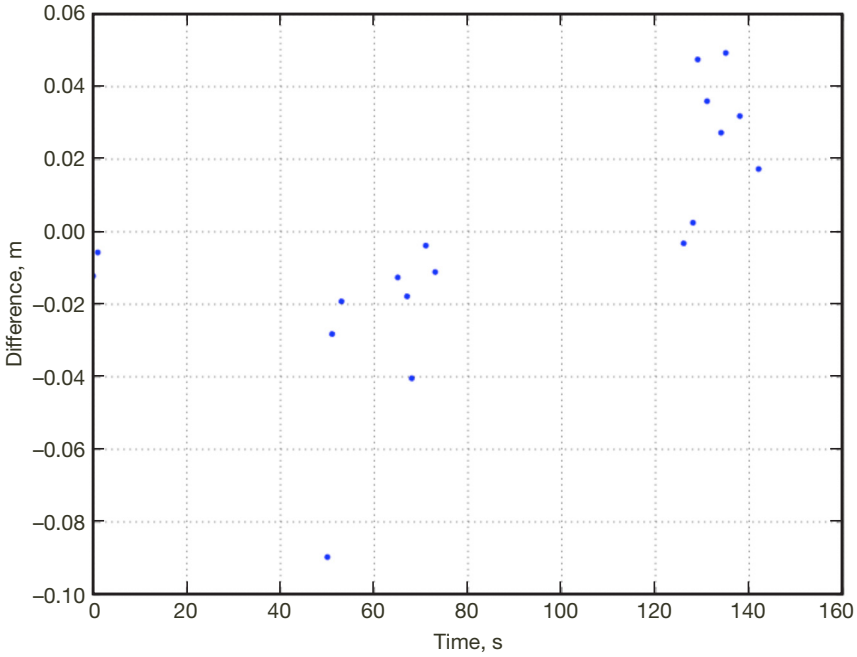

Figure 5. Difference between GPS and ALURE range estimates during the first pass.

Table 2. Error statistics by orbit number for differences between the ALURE and GPS estimates.

Track Number	Mean, cm	Std. Dev., cm	RMS, cm
4	–2.7	3.3	4.3
5	–5.9	4.2	7.2
6	–0.1	4.4	4.4
8	–9.1	5.0	10.4

VII. Summary and Conclusions

Flight test results are presented that show that the difference between the GPS and the ALURE range was on average 6.6 cm RMS. This error is consistent with the predicted experimental uncertainty of 7.73 cm. This provides strong evidence that the true uncertainty in the 3D RMS error of the PPP solution is less than 10 cm.

Of the errors presented, the most significant errors are from troposphere estimation (both from the GPS and the ALURE) and the lever arm associated with the ground stations. Improvements in experimental uncertainty will require better alignment of the ground station lever arm in the ECEF frame. In addition, combined estimation of the laser and GPS troposphere errors may yield lower uncertainty. Finally, GPS and inertial sensor fusion is known to have a lack of observability in heading angle during long, smooth flight passes. The error in heading angle may drift. A method for validating the heading angle, such as using differential GPS on the aircraft to measure attitude, should be sufficient to verify that the error in attitude is less than 0.5 deg (RMS).

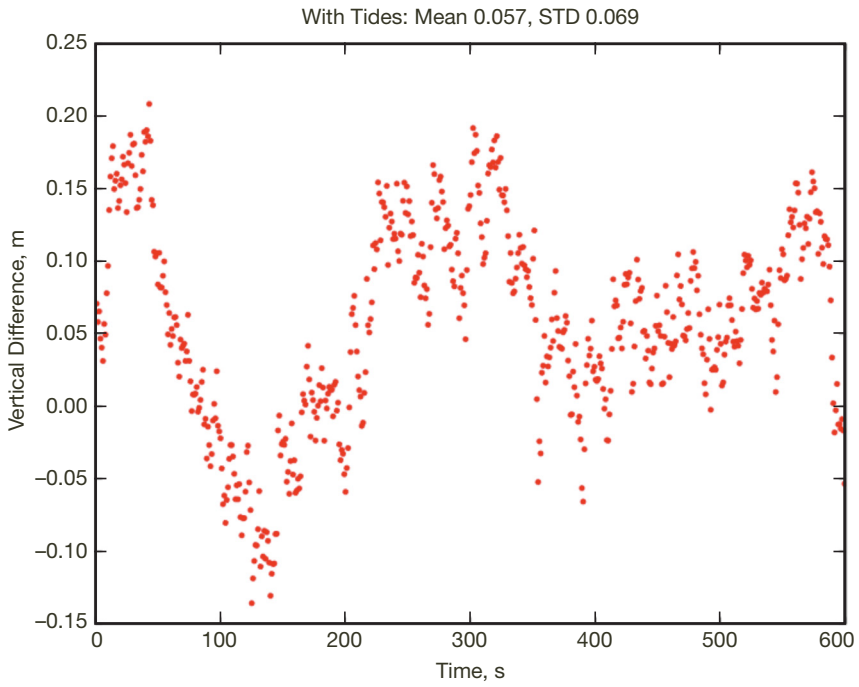

Figure 6. Difference in estimated altitude between GIPSY and annihilation method.

Table 3. Difference between annihilation method and GIPSY solution during run 4.

	Run 4		
Parameter	Mean, cm	Std. Dev., cm	RMS, cm
North	3.5	2.3	4.2
East	–5.1	1.7	5.4
Down	5.7	6.9	9
Range	10.6	3.6	11.2

In a future flight test, the authors will test the RTG processing system used on the Uninhabited Aerial Vehicle Synthetic Aperture Radar (UAVSAR) against the ALURE laser ranging system. The differences between the PPP and RTG solutions will both be compared against the ALURE in order to validate accuracy claims of 10-cm level.

The method presented is significantly different than a short-baseline kinematic method in that the results are achievable globally and without the use of a ground station. Short baseline techniques are limited in accuracy to the lateral and vertical range difference between the base station and the vehicle due to differential troposphere and ionosphere effects. The results presented here comparing PPP to the ALURE show that the estimation methods used in PPP are consistent with the laser and may be used to provide precise positioning globally.

Acknowledgments

The authors wish to acknowledge the following people for their contributions to the work for this article. First, we would like to acknowledge Robert Burtoft of IK Curtiss, the pilot and mechanic of the aircraft. Second, we wish to acknowledge Vachik Garkanian, Carlos Esproles, and Mark Thompson of JPL for their help in building and surveying the installation. Finally, the authors would like to acknowledge Shailen Desai for aiding in discussions of the use of solid-tide corrections in GIPSY processing.

References

[1] M. Armatys, R. Muellerschoen, Y. Bar-Sever, and R. Meyer, "Demonstration of Decimeter-Level Real-Time Positioning of an Airborne Platform," *Proceedings, Institute of Navigation (ION) National Technical Meeting*, Anaheim, California, January 22–24, 2003.

[2] S. Desai, W. Bertiger, B. Haines, N. Harvey, D. Kuang, C. Lane, A. Sibthorpe, F. Webb, and J. Weiss, "The JPL IGS Analysis Center: Results from the Reanalysis of the Global GPS Network," American Geophysical Union, *EOS Transactions*, vol. 90, no. 52, Fall Meeting Supplement, Abstract G11B-030, 2009.

[3] B. Haines, M. Armatys, Y. Bar-Sever, W. Bertiger, S. Desai, A. Dorsey, C. Lane, and J. Weiss, "One-Centimeter Orbits in Near-Real Time: The GPS Experience on OSTM," *Journal of the Astronautical Sciences*, vol. 58, no. 3, 2011 (accepted for publication).

[4] W. Bertiger, S. Desai, B. Haines, N. Harvey, A. Moore, S. Owen, and J. Weiss, "Single Receiver Phase Ambiguity Resolution with GPS Data," *Journal of Geodesy*, vol. 84, no. 5, pp. 327–337, March 21, 2010.

[5] W. Williamson, K. Wilson, J. Kovalik, M. Wright, B. Haines, and Y. Bar-Sever, "Comparison of Laser and Differential GPS Ranging Approaches," *The Interplanetary Network Progress Report*, vol. 42-181, Jet Propulsion Laboratory, Pasadena, California, pp. 1–14, May 15, 2010. http://ipnpr.jpl.nasa.gov/progress_report/42-181/181D.pdf

[6] J. Wolfe, W. Williamson, and J. Speyer, "Hypothesis Testing for Resolving Integer Ambiguity in GPS," *Journal of the Institute of Navigation*, vol. 50, no. 1, pp. 45–46, Spring 2003.

[7] G. Mader, "GPS Antenna Calibration at the National Geodetic Survey," National Geodetic Survey, National Oceanic and Atmospheric Administration, Silver Spring, Maryland, 2009.

[8] G. Blewitt, "An Automatic Editing Algorithm for GPS Data," *Geophysical Research Letters*, vol. 17, no. 3, pp. 199–202, March 1990.

[9] J. Kouba, "Implementation and Testing of the Gridded Vienna Mapping Function 1 (VMF1)," *Journal of Geodesy*, vol. 82, pp 193–205, 2008.

[10] D. McCarthy and G. Petit (eds.), "IERS Convention (2003)," International Earth Rotation and Reference System Service, Frankfurt, Germany, 2004.

[11] G. Blewitt, "Carrier Phase Ambiguity Resolution for the Global Positioning System Applied to Geodetic Baselines Up to 2000 km," *Journal of Geophysical Research*, vol. 94, no. B8, pp. 10187–10203, August 1999.

[12] A. E. Niell, "Global Mapping Functions for the Atmosphere Delay at Radio Wavelengths," *Journal of Geophysical Research*, vol. 101, no. B2, pp. 3227–3246, February 10, 1996.

[13] V. Mendes and E. Pavlis, "High-Accuracy Zenith Delay Predictions at Optical Wavelengths," *Geophysical Research Letters*, vol. 31, L14602, doi:10.1029/2004GL020308, 2004.

[14] W. Williamson, M. Abdel-Hafez, I. Rhee, E. Song, J. Wolfe, D. Chichka, and J. Speyer, "An Instrumentation System Applied to Formation Flight," *IEEE Transactions on Systems Technology*, vol. 15, pp. 85–88, 2007.